ACS OMEGA

http://pubs.acs.org/journal/acsodf

Article

Spectroscopic and Theoretical Investigation of β-Lactoglobulin Interactions with Hematoporphyrin and Protoporphyrin IX

Yun Wang,[#] Min Gong,[#] Zhuo Huang, Hai Min, Peng Yu, Fuzhou Tang, Yuannong Ye, Simian Zhu, Zuquan Hu, Zhu Zeng,* and Jin Chen*

Cite This: *ACS Omega* 2021, 6, 9680−9691

Read Online

ACCESS | Metrics & More | Article Recommendations | Supporting Information

ABSTRACT: Hematoporphyrin (HP) and protoporphyrin IX (PPIX) are useful porphyrin photosensitizers with significant application values in photodynamic therapy. Currently, many strategies have been developed to improve their clinical performance, such as incorporating them with nanoparticle (NP) carriers. In this work, we studied the possibility of using β-lactoglobulin (BLG) as a potential NP carrier due to their hydrophobic affinity, pH sensitivity, and low cost of extraction and preservation. The interaction mechanisms of BLG with HP and PPIX were investigated using spectroscopic techniques and molecular docking methods. The molecular docking results agree well with the experimental results, which demonstrate that the formations of HP-BLG and PPIX-BLG complexes are endothermic processes and the main acting force is hydrophobic force. Furthermore, the opening−closure states of EF loop have a great influence on the HP-BLG complex formation, where the central hydrophobic cavity of β-barrel is available for HP binding at pH 7.4 but not available at pH 6.2. However, the formation of the PPIX-BLG complex is less dependent on the states of the EF loop, and the binding sites of PPIX are both located on the external surface of BLG under both pH 7.4 and 6.2 conditions. All of our results would provide new insight into the mechanisms of noncovalent interactions between BLG and HP/PPIX. It is believed that this work indicated the potential application values of BLG in designing pH-sensitive carriers for the delivery of HP and PPIX, as well as other poorly soluble drugs.

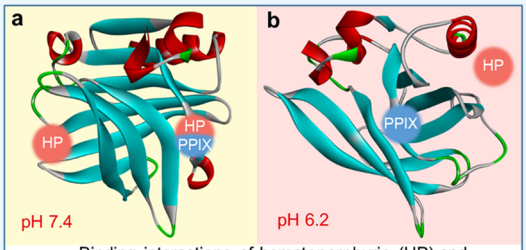

Binding interactions of hematoporphyrin (HP) and protoporphyrin IX (PPIX) to beta-lactoglobulin

1. INTRODUCTION

Porphyrins and their derivatives, as one of the photosensitizers, offer prominent potential and scope either as imaging contrast or photodynamic therapy (PDT) agents due to their good biocompatibility, high intrinsic specificity for tumors, and easy generation of reactive oxygen species.[1−3] Among many porphyrin drugs, hematoporphyrin (HP) and protoporphyrin IX (PPIX) are two typical representatives based on the porphyrin structure. HP, as the first-generation photosensitizers, is employed in early PDT, which is widely used in the clinical treatment of a variety of cancers.[1−3] PPIX is a precursor of heme and shown to have a longer wavelength absorption, which is considered as the second-generation photosensitizers and employed in PDT.[2,3] Currently, nanotechnology, incorporating nanoparticle (NP) carriers with photosensitizers, is a cutting-edge strategy to improve the performance of PDT.[3] Among many kinds of NP carriers, protein molecules with good hydrophobic affinity, for example, blood plasma-derived proteins, have a great development prospect.[4−6] From a physiological point of view, once entering the bloodstream, porphyrins and their derivatives often combine with circulating proteins (*e.g.*, low-density lipoproteins, serum albumin, and glycoproteins) to form porphyrin (or its derivatives)−protein complexes,[2] which changes the drugs' hydrophobicity/hydrophilicity and determines their affinity and avidity for tumor tissue.[2,3] However, it is expensive to extract and preserve the blood plasma-derived proteins, which limits the large-scale application of such protein carriers. Then, it is of great significance to develop inexpensive and widely available proteins as carriers or part of carriers. Additionally, given that most porphyrins and their derivatives are site nonspecific drugs for tumor tissue[7,8] and that the pH value of the tumor microenvironment (pH 5.8−7.4) is different from that of the normal extracellular microenvironment (pH ≈ 7.4),[9,10] the pH-sensitive proteins might be one of the ideal carriers, which is conducive to control the release of these drugs in the tumor microenvironment.

Bovine β-lactoglobulin (BLG), containing 162 amino acid residues with a molecular mass of 18.3 kDa and a diameter of ∼6 nm, is soluble and constitutes 7−12% of total milk

Received: January 16, 2021
Accepted: March 24, 2021
Published: April 1, 2021

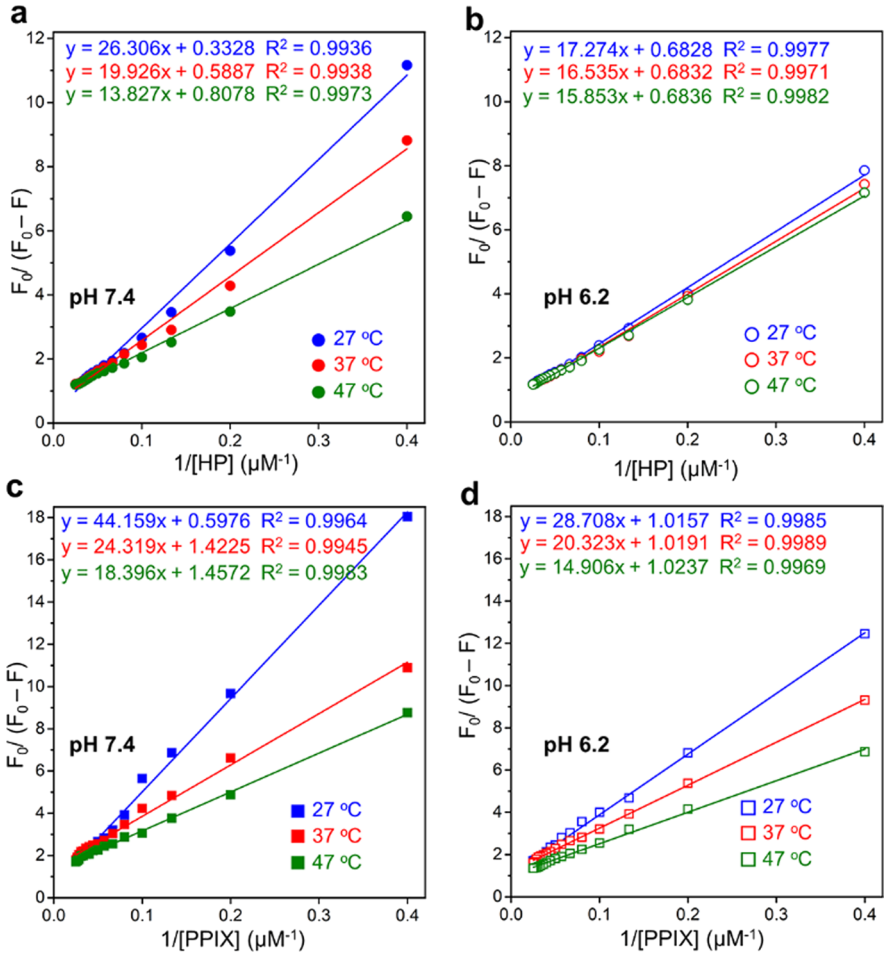

Figure 1. Modified Stern−Volmer plots of BLG (5 μM) interaction with HP or PPIX at temperatures of 27, 37, and 47 °C. (a) HP, at pH 7.4; (b) HP, at pH 6.2; (c) PPIX, at pH 7.4; (d) PPIX, at pH 6.2.

proteins.[11] The secondary structure of BLG consists of nine antiparallel β-strands (strands A−I) and one α-helix, in which strands A−H fold up into a flattened β-barrel with seven connection loops labeled as AB, BC, CD, DE, EF, FG, and GH, respectively.[12−14] BLG belongs to the lipocalin protein superfamily and usually contains three main regions for interacting with hydrophobic ligands, including the central hydrophobic cavity of the β-barrel, the surface hydrophobic pocket in a groove between the α-helix and the β-barrel, and the external surface near the bottom of the β-barrel.[12−14] Many studies have proven the excellent abilities of BLG in binding and transporting a great variety of amphiphilic and hydrophobic agents or drugs.[15−18] Moreover, among the binding regions of BLG, the accessibility of the central hydrophobic cavity of the β-barrel is dependent on pH values. EF loop works as a gate over the binding site, and its reversible opening−closure can prevent ligand binding below pH 7.1 but allows it at higher pH values.[13,17,19] Hence, BLG could be employed as a pH-sensitive transport vector for drugs, such as porphyrins and their derivatives, whose delivery and release is required to depend on physiological environments.[16,20,21] However, the mechanisms of noncovalent interactions between porphyrins (or their derivatives) and BLG, especially the possible mechanism differences under different pH conditions, remain to be investigated, which are critical to the potential of using BLG for drug delivery but often overlooked.

In this work, we sought to explore the possibility of using BLG as a carrier (or part of a carrier) for HP and PPIX, two kinds of classical porphyrins. To this end, various spectroscopic techniques and molecular docking methods were implemented to investigate the interactions of HP and PPIX with BLG at alkaline and acidic conditions (pH 7.4 and 6.2). Our results demonstrate that both HP and PPIX can combine with BLG to form stable complexes. Their formation processes are endothermic, and the main acting force is hydrophobic force. Furthermore, our data also show that BLG is pH-sensitive and pH values have a great influence on the combination mode of the HP-BLG complex, in which the central hydrophobic cavity of the β-barrel is available for HP binding at pH 7.4 but not available at pH 6.2. Unlike the HP-BLG complex, the formation of the PPIX-BLG complex is less dependent on the effects of pH values on the BLG structure, and the main hydrophobic binding sites are located on the external surface of BLG under pH 7.4 and 6.2 conditions. It is believed that our findings will contribute to an in-depth understanding of the binding mechanisms of BLG with HP and PPIX and provide a theoretical basis for the following BLG-based carrier design and its applications in the delivery of poorly soluble drugs.

2. RESULTS AND DISCUSSION

2.1. Fluorescence Quenching Mechanism. Fluorescence quenching analysis is a powerful and accurate method to investigate molecular interactions.[19,22] Previous studies have

https://doi.org/10.1021/acsomega.1c00279
ACS Omega 2021, 6, 9680−9691

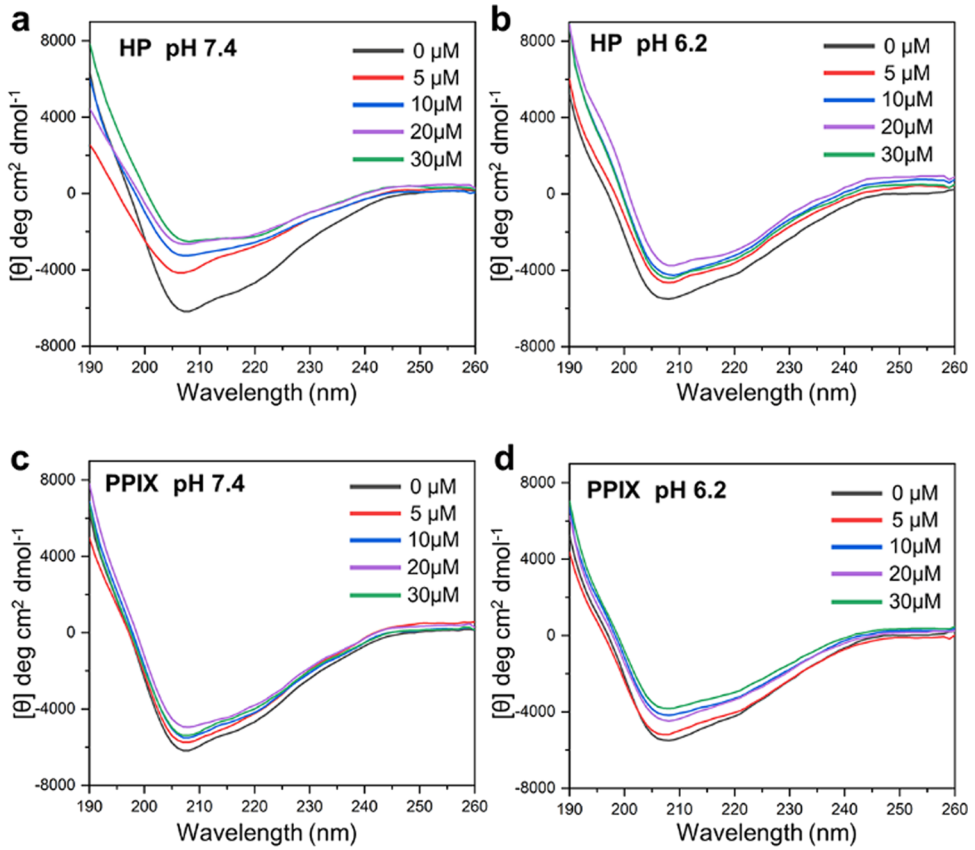

Figure 2. Circular dichroism spectra of BLG (5 μM) in the absence and presence of HP or PPIX at various concentrations (0, 5, 10, 20, and 30 μM) at 37 °C. (a) HP, at pH 7.4; (b) HP, at pH 6.2; (c) PPIX, at pH 7.4; (d) PPIX, at pH 6.2.

shown that a BLG monomer has two tryptophan (Trp-19 and Trp-61) residues and four tyrosine (Tyr-20, Trp-42, Trp-99, and Trp-101) residues, which can possess intrinsic fluorescence.[19,23] Given that the 280 nm light can excite both Trp and Tyr residues,[19,23,24] herein, BLG solutions were excited at 280 nm and the emission spectra of wavelength at 300−500 nm were recorded in the absence and presence of different concentrations of HP and PPIX. As shown in Figure S1, with increasing concentrations of HP and PPIX, the fluorescence intensity of BLG decreases gradually, manifesting that the interactions of HP and PPIX with BLG lead to fluorescence quenching. To analyze the fluorescence quenching contributions of Trp and Tyr residues, synchronous fluorescence studies were applied by setting $\Delta\lambda$ at 60 nm for Trp and 15 nm for Tyr.[25,26] As shown in Figure S2, the synchronous fluorescence intensity of each BLG sample at $\Delta\lambda$ = 60 nm shows a stronger intensity than that at $\Delta\lambda$ = 15 nm, indicating that Trp residues are dominant in the total fluorescence emission. Additionally, with increasing HP/PPIX concentrations, the quenching degree of fluorescence intensity of each BLG sample at $\Delta\lambda$ = 60 nm is much more obvious than that at $\Delta\lambda$ = 15 nm. These results suggest that the Trp residues are mainly responsible for the fluorescence quenching instead of Tyr residues. It is worth noting that, for the intrinsic fluorescence of Trp residues, the contribution from Trp-19 is superior to that from Trp-61[27] because Trp-19 is located on an apolar environment while Trp-61 is partly exposed to an aqueous solvent.[28]

To shed light on the quenching mechanism, the fluorescence emission spectra of BLG solutions with different concentrations of HP and PPIX at different temperatures (27, 37, and 47 °C) and different pH conditions (7.4 and 6.2) were recorded. Then, the modified Stern−Volmer equations (eqs 1 and 2) were applied to calculate the fluorescence quenching parameters:[29,30]

$$\frac{F_0}{F_0 - F} = \frac{1}{K_{sv} f_a} \frac{1}{[C]} + \frac{1}{f_a} \quad (1)$$

$$K_{sv} = K_q \tau_0 \quad (2)$$

F_0 and F are the maximum fluorescence intensities in the absence and presence of a quencher (HP or PPIX), and [C] is the concentration of a quencher. K_{sv} is the Stern−Volmer quenching constant, and its value is the quotient of f_a^{-1} and $(f_a K_{sv})^{-1}$. K_q is the biomolecular quenching rate constant, which is a key index for determining whether the fluorescence quenching mechanism is static or dynamic.[14,28,30] τ_0 is the fluorescence average lifetime of the fluorophore and has been reported to be 1.28 ns for the Trp residues of BLG.[23,31]

As shown in Figure 1, for all groups, the dependences of $F_0/(F_0 - F)$ on the reciprocal value of the quencher concentration $[C]^{-1}$ are linear. Then, the detailed K_{sv} and K_q values of each group could be calculated and the corresponding results are listed in Tables S1 and S2. For the interaction of HP with BLG, the K_q value is from 9.884×10^{12} to 45.642×10^{12} M^{-1} s^{-1} at pH 7.4 and from 30.881×10^{12} to 33.688×10^{12} M^{-1} s^{-1} at pH 6.2. Given that the maximal K_q value of dynamic quenching constant is just 2.0×10^{10} M^{-1} s^{-1},[14,28,30] the K_q value of the interaction of HP with BLG suggests that the dominant mechanism of fluorescence quenching is static rather

https://doi.org/10.1021/acsomega.1c00279
ACS Omega 2021, 6, 9680−9691

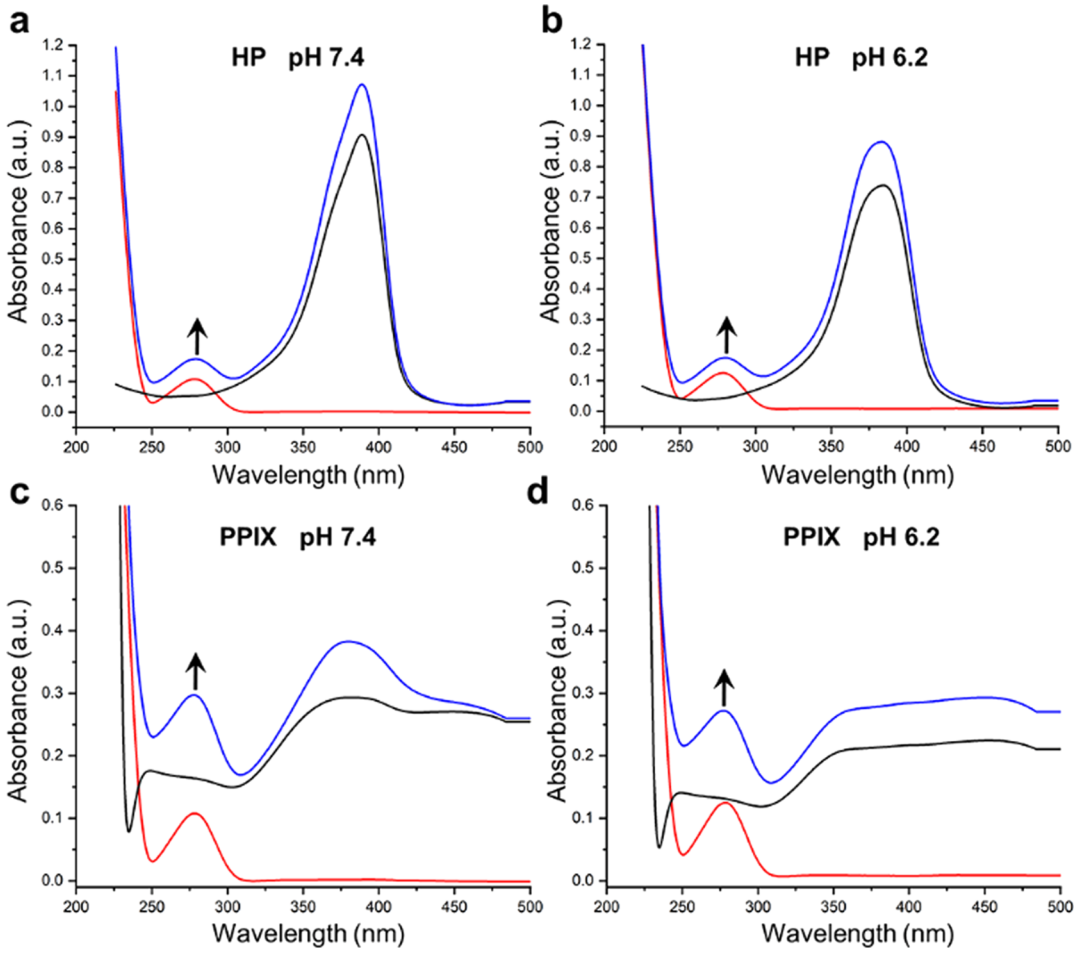

Figure 3. UV−vis absorption spectra of BLG (5 μM) in the absence and presence of HP or PPIX at 37 °C. (a) 5 μM HP, at pH 7.4; (b) 5 μM HP, at pH 6.2; (c) 30 μM PPIX, at pH 7.4; (d) 30 μM PPIX, at pH 6.2.

than dynamic.[14,28,30] Namely, the fluorescence quenching is mainly caused by the formation of the HP-BLG complex instead of dynamic collision. For the interaction of PPIX with BLG, the K_q value is from 10.572×10^{12} to 61.885×10^{12} M^{-1} s^{-1} at pH 7.4 and from 27.641×10^{12} to 53.654×10^{12} M^{-1} s^{-1} at pH 6.2, which is also much higher than the maximal dynamic quenching constant. It suggests that static quenching is dominant, meaning that the formation of the PPIX-BLG complex is mainly responsible for the fluorescence quenching.

It is worth noting that, with increasing temperature, the K_{sv} value of the HP-BLG complex increases evidently from 12.651×10^3 to 58.422×10^3 M^{-1} at pH 7.4 but does not show noticeable change (just from 39.528×10^3 to 43.121×10^3 M^{-1}) at pH 6.2 (Table S1). According to previous studies proposing that the EF loop of BLG can act as a gate over the central hydrophobic cavity of the β-barrel (Figure S3), which open at pH > 7.1 and close at pH < 7.1,[13,16,17,19] the K_{sv} variation degree of the HP-BLG complex under different pH conditions suggests that the formation efficiency of the HP-BLG complex could depend on the effects of pH values on the BLG structure. However, the K_{sv} variation degree of the PPIX-BLG complex under different pH conditions (Table S2) is different from that of the HP-BLG complex, which increases evidently both at pH 7.4 (from 13.533×10^3 to 79.213×10^3 M^{-1}) and at pH 6.2 (from 35.380×10^3 to 68.677×10^3 M^{-1}). This indicates that the effects of pH values on the BLG structure may have little influence on the formation efficiency of the PPIX-BLG complex.

2.2. Circular Dichroism (CD) and UV−vis Studies. According to previous studies, bindings of ligands to proteins usually lead to the changes in the secondary structure.[12,32,33] Then, to figure out the conformational changes of BLG after its interactions with HP and PPIX, CD analysis was applied to characterize the secondary structure of BLG with different ratios of HP as well as PPIX. The results of CD spectra presented in Figure 2 imply that the interactions of both HP and PPIX with BLG can induce a few conformational changes in the structure of BLG. Moreover, the detailed contents of secondary structure elements of each sample were calculated using the recorded CD spectra data. For the interaction of HP with BLG (as listed in Table S3), the proportion of the α-helix decreases and the proportion of the β-sheet increases in the presence of HP under both pH 7.4 and 6.2 conditions. Furthermore, the content of the random coil structure increases slightly when the HP concentration exceeds 10 μM. For the interaction of PPIX with BLG (as listed in Table S4), in the presence of PPIX, the proportions of both the α-helix and the β-sheet seem to be unchanged at pH 7.4 but slightly decrease at pH 6.2. Additionally, the content of the random coil structure increases slightly when the HP concentration reaches to 30 μM at pH 7.4 or exceeds 10 μM at pH 6.2.

https://doi.org/10.1021/acsomega.1c00279
ACS Omega 2021, 6, 9680−9691

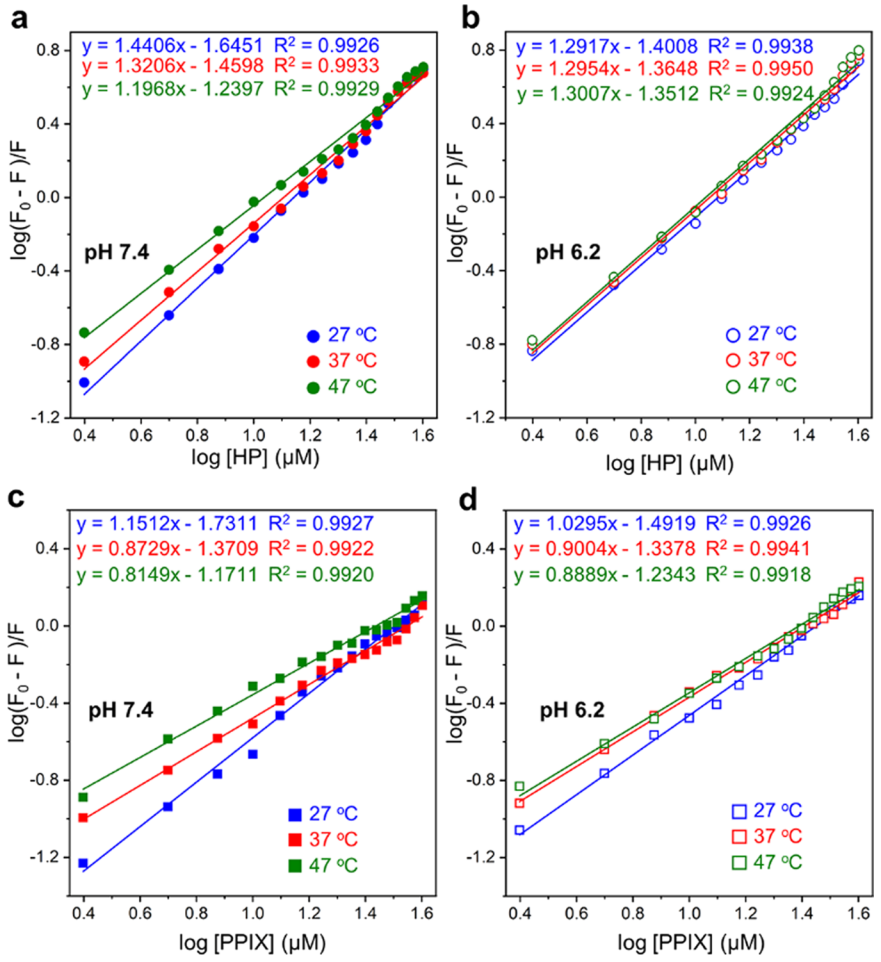

Figure 4. Curves of $\log[(F_0 - F)/F]$ *vs* $\log[C]$ of BLG interaction with HP or PPIX at temperatures of 27, 37, and 47 °C. (a) HP, at pH 7.4; (b) HP, at pH 6.2; (c) PPIX, at pH 7.4; (d) PPIX, at pH 6.2.

The UV−vis absorption spectrum is an easy and effective tool to evaluate the structural changes during the complex formation between ligands and protein. Then, to confirm the results of the fluorescence quenching and CD studies, UV−vis experiments were also performed. As shown in Figure 3, both HP and PPIX do not have obvious absorption peaks at 280 nm. After the addition HP or PPIX, the absorbance intensity of each BLG solution sample at 280 nm is significantly increased under both pH 7.4 and 6.2 conditions, suggesting conformational changes in the structure of BLG. Given that the UV−vis absorption spectrum is altered in a static quenching mechanism but not altered in a dynamic quenching mechanism,[25,34,35] it can be inferred that the dominant fluorescence quenching mechanism of BLG by HP/PPIX is a static quenching procedure. All the above results indicate that the complex formations are the outcomes of the interactions between BLG and HP/PPIX, resulting in fluorescence quenching *via* a static quenching mechanism.

2.3. Thermodynamic Analysis. According to previous reports, in the case of static quenching models, the binding parameters of the ligand−protein complexes could be calculated using eq 3.[36] K_b is the binding constant, and n is the average number of ligands binding to per protein molecule.

$$\log\left[\frac{F_0 - F}{F}\right] = \log K_b + n \log[C] \quad (3)$$

As shown in Figure 4, for all groups, the dependences of $\log[(F_0 - F)/F]$ on the ligand concentration [C] are linear. The detailed K_b and n values of each group could be calculated, and the corresponding results are listed in Tables S5 and S6. It can be seen that, with increasing temperature, the K_b value of the HP-BLG complex markedly increases from 22.641×10^3 to 57.584×10^3 M^{-1} at pH 7.4 but only shows a little enhancement from 39.737×10^3 to 44.545×10^3 M^{-1} at pH 6.2 (Table S5). As listed in Table S6, the K_b value of the PPIX-BLG complex obviously increases from 18.574×10^3 to 67.437×10^3 M^{-1} at pH 7.4, which is similar to that of the HP-BLG complex at pH 7.4. However, the K_b value of the PPIX-BLG complex also shows evident enhancement from 32.211×10^3 to 58.304×10^3 M^{-1} at pH 6.2, which is different from that of the HP-BLG complex at pH 6.2. With increasing temperature, the enhanced K_b value reveals that the formations of both HP-BLG and PPIX-BLG are affected by heat, suggesting that their formation processes may be endothermic. Furthermore, under pH 6.2 conditions, the different K_b variation degrees between the HP-BLG complex and PPIX-BLG complex also indicate that the effects of pH values on the BLG structure should have different impacts on the formations of these two complexes.

Given that the thermodynamic parameters are the main criteria to estimate binding modes,[32,37,38] the Gibbs free energy (ΔG), enthalpy change (ΔH), and entropy change (ΔS) of the HP-BLG and PPIX-BLG complex were evaluated using the van't Hoff equation (eq 4)[34,35] in order to better figure out the

https://doi.org/10.1021/acsomega.1c00279
ACS Omega 2021, 6, 9680−9691

Table 1. Thermodynamic Parameters of the HP-BLG Complex ΔG (kJ mol^{-1})

	pH = 7.4			pH = 6.2		
temp (°C)	ΔG (kJ mol^{-1})	ΔH (kJ mol^{-1})	ΔS (kJ mol^{-1})	ΔG (kJ mol^{-1})	ΔH (kJ mol^{-1})	ΔS (kJ mol^{-1})
27	−25.011	37.299	0.208	−26.412	4.537	0.103
37	−26.944			−27.508		
47	−29.162			−28.478		

Table 2. Thermodynamic Parameters of the PPIX-BLG Complex

	pH = 7.4			pH = 6.2		
temp (°C)	ΔG (kJ mol^{-1})	ΔH (kJ mol^{-1})	ΔS (kJ mol^{-1})	ΔG (kJ mol^{-1})	ΔH (kJ mol^{-1})	ΔS (kJ mol^{-1})
27	−24.517	51.318	0.253	−25.890	23.638	0.165
37	−27.471			−27.668		
47	−29.582			−29.194		

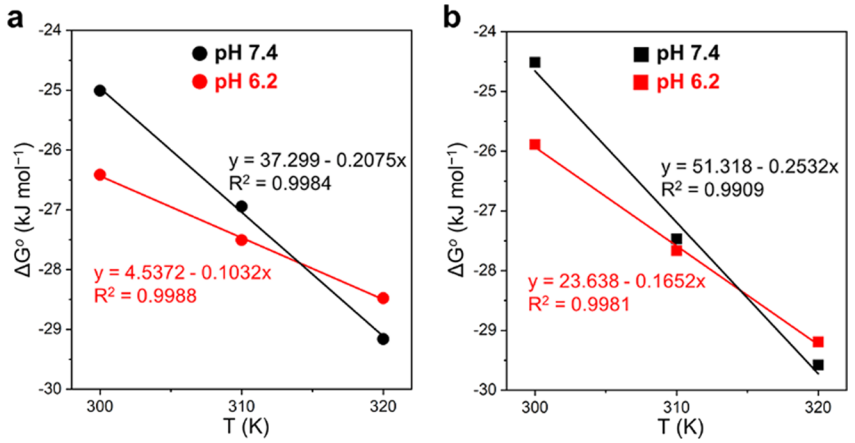

Figure 5. ΔG *vs* T (thermodynamic temperature) plots of BLG interaction with (a) HP and (b) PPIX at pH 7.4 and 6.2.

forces acting between ligands and the BLG protein. T is the thermodynamic temperature, and R is the gas constant. K_b is the binding constant at a corresponding temperature, which is obtained from eq 3 and listed in Tables S5 and S6.

$$\Delta G = -RT\ln K_b = \Delta H - T\Delta S \quad (4)$$

The calculated ΔG value of each group is summarized in Tables 1 and 2. For both HP-BLG and PPIX-BLG complexes, the negative sign for ΔG implies that their formation processes are spontaneous.[28] As shown in Figure 5, the dependences of ΔG on the thermodynamic temperature T are linear. Thus, the ΔH and ΔS of the HP-BLG and PPIX-BLG complex formations could be computed (Tables 1 and 2), which can roughly predict the main four types of noncovalent forces stabilizing ligand−protein complexes: (a) $\Delta H > 0$ and $\Delta S > 0$, hydrophobic force; (b) $\Delta H < 0$ and $\Delta S < 0$, van der Waals force or hydrogen bonds; and (c) $\Delta H < 0$ and $\Delta S > 0$, electrostatic interactions.[32,37,38]

For the HP-BLG complex, the ΔH and ΔS values are 37.299 and 0.208 kJ mol^{-1} at pH 7.4 and 4.537 and 0.103 kJ mol^{-1} at pH 6.2, respectively. These positive ΔH and ΔS values indicate that the main acting force of the HP-BLG complex is hydrophobic force. For the PPIX-BLG complex, the ΔH and ΔS values are 51.318 and 0.253 kJ mol^{-1} at pH 7.4 and 23.638 and 0.165 kJ mol^{-1} at pH 6.2, respectively. It means that hydrophobic force also plays a major role in the formations of the PPIX-BLG complex.

Furthermore, it is worth noting that the ΔH and ΔS values of the HP-BLG complex at pH 6.2 decrease obviously in comparison with those of the HP-BLG complex at pH 7.4, suggesting weakened hydrophobic force between HP and BLG.[38,39] This interesting phenomenon might be caused by the closed EF loop at pH < 7.1,[13,19] which hinders HP from entering the central hydrophobic cavity of the β-barrel. On the other hand, although the ΔH and ΔS values of the PPIX-BLG complex decrease with the shift of pH value from 7.4 to 6.2, the decrease degrees are less than those of HP-BLG. It means that the formation of the PPIX-BLG complex is less dependent on the accessibility of the central hydrophobic cavity of the β-barrel (*i.e.*, closed/opened EF loop) than that of the HP-BLG complex.

2.4. Fluorescence Resonance Energy Transfer (FRET) Studies. As previously mentioned, for the intrinsic fluorescence of Trp residues, Trp-19 is the major contributor to the fluorescence emission.[27,28] According to Förster's theory,[40] FRET is a useful method to estimate the distance (r_0) between the donor (in this case Trp-19 of BLG) and the acceptor (in this case HP or PPIX), following eqs 5 and 6. E is the efficiency of energy transfer between the donor and the acceptor, R_0 is the critical distance when the transfer efficiency is 50%, K^2 is the orientation factor, N is the refractive index of the medium, and φ is the fluorescence quantum yield of the donor. According to previous reports,[21,28] the values of K^2, N, and φ are 2/3, 1.336, and 0.08, respectively. J is the spectral overlap integral between the emission spectrum of the donor and the absorption spectrum of the acceptor, which can be calculated by following eq 7.[25,26] $F(\lambda)$ and $\varepsilon(\lambda)$ represent the

https://doi.org/10.1021/acsomega.1c00279
ACS Omega 2021, 6, 9680−9691

Table 3. Overlap Integral (J), Critical Distance (R_0), and Donor−Acceptor Distance (r_0) of the HP-BLG Complex and PPIX-BLG Complex at 37 °C

	pH = 7.4			pH = 6.2		
complex	J ($\times 10^{-13}$ cm^3 M^{-1})	R_0 (nm)	r_0 (nm)	J ($\times 10^{-13}$ cm^3 M^{-1})	R_0 (nm)	r_0 (nm)
HP-BLG	1.121	3.47	4.58	1.288	3.52	4.80
PPIX-BLG	0.114	2.35	3.44	0.070	2.17	3.09

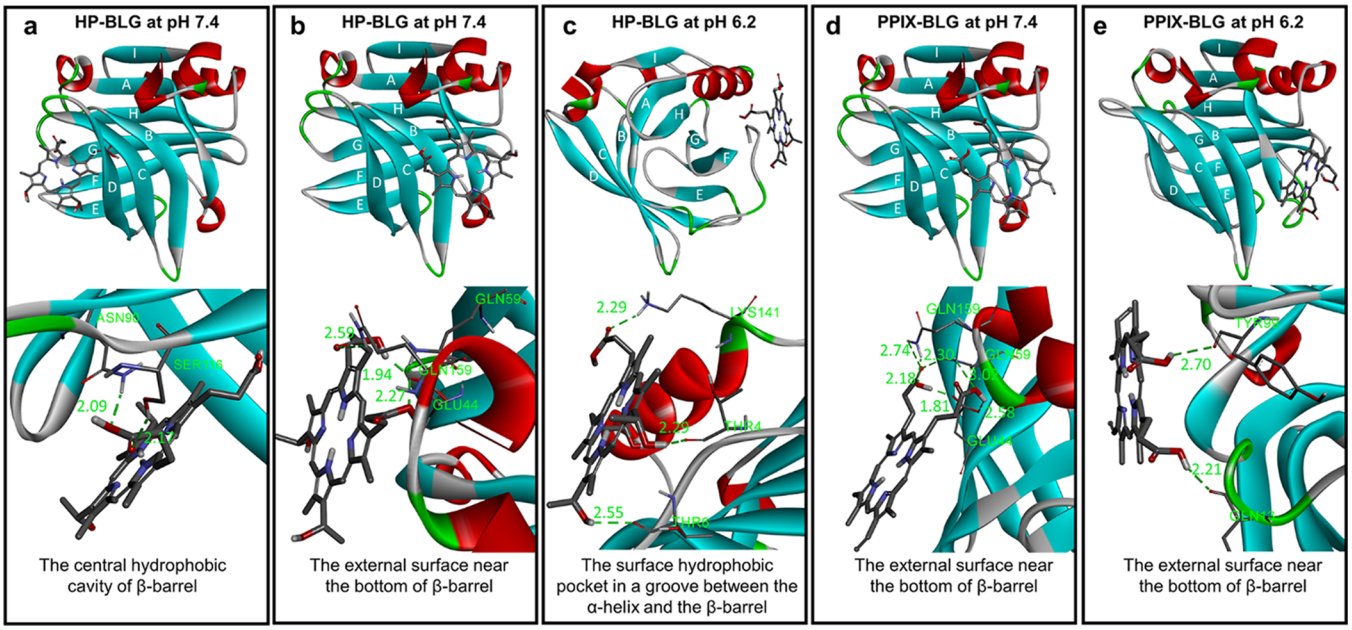

Figure 6. Molecular docking analysis of the binding sites. The BLG is represented in a ribbon model, and the ligands are represented in a stick model. (a, b) HP-BLG complex at pH 7.4; (c) HP-BLG complex at pH 6.2; (d) PPIX-BLG complex at pH 7.4; (e) PPIX-BLG complex at pH 6.2.

fluorescence intensity of the donor and the molar extinction coefficient of the acceptor, respectively.

$$E = 1 - \frac{F}{F_0} = \frac{R_0^6}{R_0^6 + r_0^6} \tag{5}$$

$$R_0^6 = 8.79 \times 10^{-25} K^2 N^{-4} \varphi J \tag{6}$$

$$J = \frac{\sum F(\lambda)\varepsilon(\lambda)\lambda^4 \Delta\lambda}{\sum F(\lambda)\Delta\lambda} \tag{7}$$

The fluorescence emission spectra of BLG (5 μM) and the UV−vis absorption spectra of HP (5 μM) and PPIX (5 μM) at 37 °C are displayed in Figure S4. Then, the J value is calculated by integration of the overlapping spectra in a wavelength of 290−440 nm, and the R_0 and r_0 values could be computed. As listed in Table 3, the R_0 and r_0 of the HP-BLG complex are 3.47 and 4.58 nm at pH 7.4, and 3.52 and 4.80 nm at pH 6.2, respectively. Meanwhile, the R_0 and r_0 of the PPIX-BLG complex are 2.35 and 3.44 nm at pH 7.4 and 2.17 and 3.09 nm at pH 6.2, respectively. According to Förster's theory and previous reports, the condition of non-radioactive energy transfer is 0.5 $R_0 < r_0 < 1.5\ R_0$,[41] and $R_0 < r_0 < 8$ nm is a strong evidence for static quenching.[42] Thus, the r_0 and corresponding R_0 values of each sample not only reveal that resonance energy transfer occurs between HP/PPIX and BLG but also confirm that static quenching is dominant in these quenching processes, which is in line with the hypothesis mentioned in the above section (*i.e.*, fluorescence quenching mechanism).

Moreover, it is worth noting that, with the shift of pH value from 7.4 to 6.2, the r_0 value of HP-BLG becomes larger (from 4.58 to 4.80 nm) but that of PPIX-BLG becomes smaller (from 3.44 to 3.09 nm). These results indicate that the exposed β-barrel caused by opening the EF loop is a closer and available site for HP binding but not for PPIX binding. Namely, the access to the central hydrophobic cavity of the β-barrel is a pivotal way for BLG to bind with HP but not with PPIX.

2.5. Molecular Docking Results. To detail binding sites of the HP-BLG complex and PPIX-BLG complex, molecular docking was performed using AutoDock Vina and the results were analyzed using Discovery Studio. Given that previous studies have reported three binding sites of BLG: the central hydrophobic cavity of the β-barrel, the surface hydrophobic pocket in a groove between the α-helix and the β-barrel, and the external surface near the bottom of the β-barrel,[20,23,43] herein, the molecular docking was performed by approaching HP and PPIX molecules to these three sites under the condition of pH 7.4 and 6.2, respectively.

For the HP-BLG complex, the molecular docking results show that the EF loop opens the entrance to the β-barrel at pH 7.4, and these three sites could produce stable binding configurations with diverse energy minima: −28.01 kJ mol^{-1} for the central hydrophobic cavity of the β-barrel, −28.42 kJ mol^{-1} for the external surface near the bottom of the β-barrel, and −22.41 kJ mol^{-1} for the surface hydrophobic pocket in a groove between the α-helix and the β-barrel. Obviously, the central hydrophobic cavity of the β-barrel and the external surface near the bottom of the β-barrel are two main sites for binding HP at pH 7.4, which are selected to explore the

https://doi.org/10.1021/acsomega.1c00279
ACS Omega 2021, 6, 9680−9691

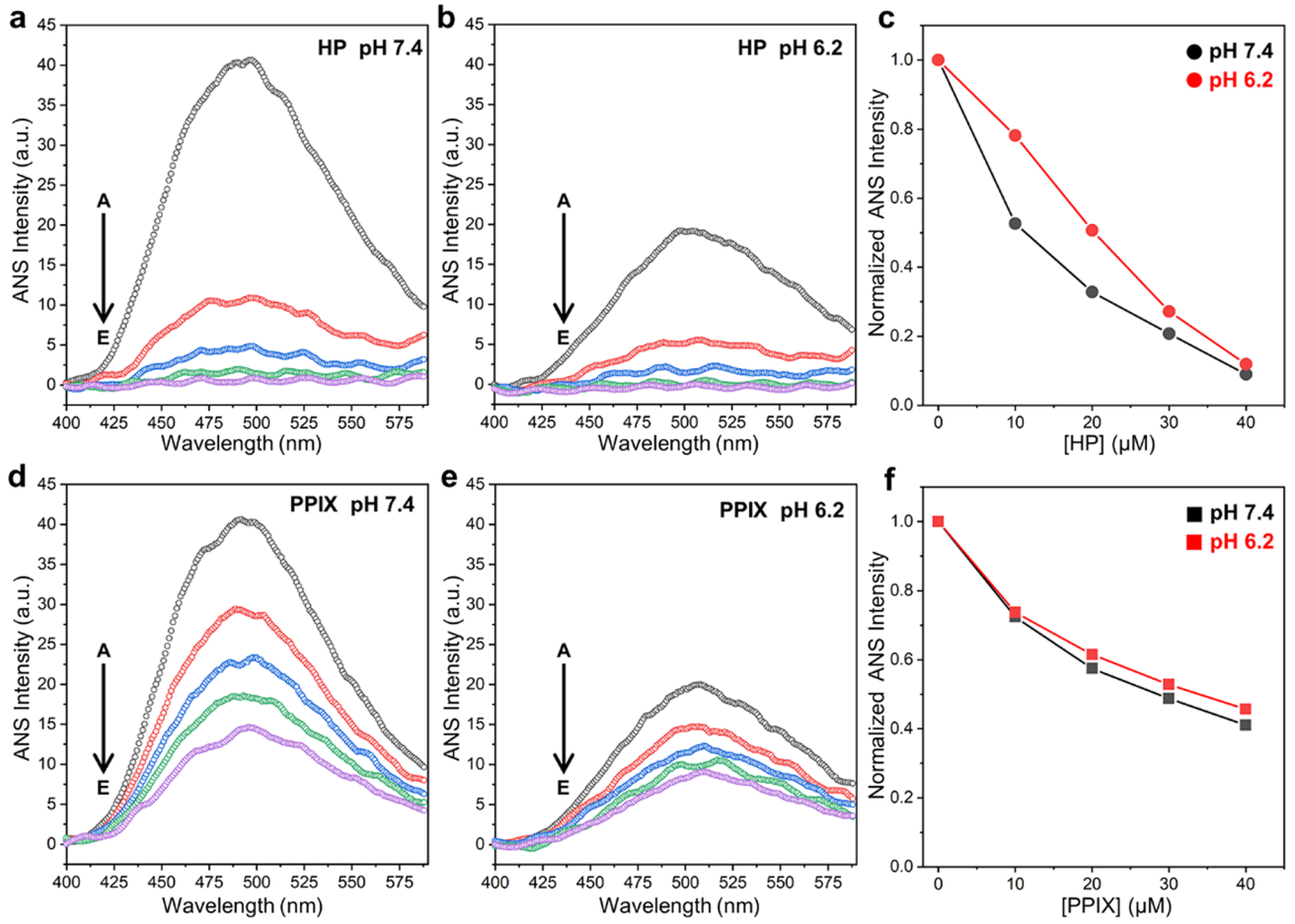

Figure 7. ANS emission of BLG (5 μM) upon increasing the concentrations of HP or PPIX (A = 0, B = 10, C = 20, D = 30, and E = 40 μM) at 37 °C. (a) HP, at pH 7.4; (b) HP, at pH 6.2; (c) normalized results of the maximum ANS emission intensity in panels (a) and (b). (d) PPIX, at pH 7.4; (f) PPIX, at pH 6.2; (f) normalized results of the maximum ANS emission intensity in panels (d) and (e).

conformations of HP-BLG. As shown in Figure 6a and Figure S5a, the HP molecule located within the central hydrophobic cavity of the β-barrel is adjacent to Pro-38, Asn-90, Asn-88, Asn-109, Ser-116, Leu-39, Met-107, Ile-56, Val-41, Leu-58, Asp-85, Ile-71, Ile-72, Lys-69, Lys-70, and Phe-105 residues. Among them, a lot of amino acids are hydrophobic, such as Pro-38, Leu-39, Met-107, Ile-56, Val-41, Leu-58, Ile-71, Ile-72, and Phe-105. Meanwhile, Figure 6b and Figure S5b display that the HP molecule located on the external surface near the bottom of the β-barrel is surrounded by Lys-47, Leu-57, Gln-68, Glu-44, Gln-159, Glu-158, Gln-59, Glu-157, Tyr-20, and Thr-18 residues, in which Leu-57 is hydrophobic. On the other hand, the simulation analysis indicates that the central hydrophobic cavity of the β-barrel cannot yield energetically favorable conformation for HP binding at pH 6.2, resulting in only two stable binding sites. The main reason might be the case that the EF loop closes the access to the β-barrel under acidic conditions,[13,16,17,19] blocking the entrance of the HP. For these two available binding sites, the HP molecule located on the surface hydrophobic pocket in a groove between the α-helix and the β-barrel (-27.17 kJ mol^{-1}) is more stable than that on the external surface near the bottom of the β-barrel (-25.92 kJ mol^{-1}). Figure 6c and Figure S5c display that the HP molecule located on the surface hydrophobic pocket in a groove between the α-helix and the β-barrel is surrounded by Thr-4, Lys-8, Thr-6, Gln-5, Asp-96, Lys-135, Ala-139, Leu-104, and Lys-141 residues, in which Ala-139 and Leu-104 are hydrophobic.

For the PPIX-BLG complex, the molecular docking results show similar outcomes in docking PPIX under pH 7.4 and 6.2 conditions, in which the central hydrophobic cavity of the β-barrel cannot yield an energetically favorable conformation. For other two binding sites, the PPIX molecule located on the external surface near the bottom of the β-barrel (-29.26 kJ mol^{-1} at pH 7.4 and -29.678 kJ mol^{-1} at pH 6.2) is more stable than that on the surface hydrophobic pocket in a groove between the α-helix and the β-barrel (-26.33 kJ mol^{-1} at pH 7.4 and -25.08 kJ mol^{-1} at pH 6.2). Figure 6d and Figure S6a display that the PPIX molecule located on the external surface near the bottom of the β-barrel is surrounded by Lys-47, Leu-57, Gln-68, Gln-159, Gln-59, Glu-44, Glu-158, Leu-156, His-161, Glu-157, Tyr-20, and Thr-18 residues at pH 7.4, in which Leu-57 and Leu-156 are hydrophobic amino acids. Meanwhile, Figure 6e and Figure S6b show that PPIX is adjacent to Thr-18, Gly-17, Ala-16, Lys-14, Gln-13, Val-15, Tyr-99, Lys-100, Thr-125, and Tyr-20 residues at pH 6.2, in which Gly-17, Ala-16, and Val-15 are hydrophobic. All the above results indicated that hydrophobic interactions might contribute to the stability of the HP-BLG complex and PPIX-BLG complex, which is consistent with the results of the thermodynamic analysis (Figure 5 and Tables 1 and 2).

Moreover, the formation of the HP-BLG complex is affected by pH conditions, in which the opened EF loop (at pH 7.4)

https://doi.org/10.1021/acsomega.1c00279
ACS Omega 2021, 6, 9680−9691

can provide entrance for HP to bind the central hydrophobic cavity of the β-barrel. On the other hand, the formation of the PPIX-BLG complex is less dependent on pH values (*i.e.*, closed/opened EF loop) because the binding sites of PPIX to BLG are mainly located on the external surface sites of BLG (*e.g.*, the external surface near the bottom of the β-barrel).

2.6. ANS (8-Anilino-1-naphthalenesulfonate) Binding Analysis. ANS is a molecule with both hydrophilic and hydrophobic properties, which is an excellent tool to reflect ligand−protein interactions *via* its fluorescence changes.[44,45] Usually, BLG can possess two binding sites for ANS: an external site that is close to a hydrophobic patch on the protein surface and an internal site that is located in the hydrophobic β-barrel of the protein.[30,44] Herein, ANS (120 μM) was used to further characterize the hydrophobic interactions in the formations of the HP-BLG complex and PPIX-BLG complex. The solution of each group was excited at 380 nm, and the emission spectra of wavelength at 400−600 nm were recorded. As shown in Figure 7, the ANS fluorescence intensity of BLG alone shows an obvious decrease with the shift of pH value from 7.4 to 6.2, suggesting that EF loop states would control the access to the central hydrophobic cavity of the β-barrel and impact the interaction of ANS with BLG.

For the HP-BLG complex, the ANS fluorescence intensity shows an evident decrease with increasing the ratio of HP under both pH 7.4 and 6.2 conditions (Figure 7a,b). Furthermore, Figure 7c shows that the decrease degree of ANS fluorescence intensity at pH 7.4 conditions is much larger than that at the 6.2 condition (especially at 10 and 20 μM HP). These results indicate that hydrophobic force is the main acting force of the HP-BLG complex and HP can compete with ANS for hydrophobic site binding, especially for the central hydrophobic cavity of the β-barrel under the opened state of the EF loop (pH 7.4).

For the PPIX-BLG complex, under both pH 7.4 and 6.2 conditions, increasing the ratio of PPIX can also cause decreases in ANS fluorescence intensity (Figure 7d,e), indicating the pivotal role of hydrophobic force in the formations of the PPIX-BLG complex. Additionally, the decrease degree of ANS fluorescence intensity at pH 7.4 conditions is similar to that at pH 6.2 conditions (Figure 7f), suggesting that the competition between PPIX and ANS is less affected by the EF loop state (*i.e.*, opened or closed). Namely, the main binding sites of PPIX with BLG are located on the external surface instead of the internal hydrophobic region (*i.e.*, the central hydrophobic cavity of the β-barrel), which is in line with the results of molecular docking (Figure 6 and Figure S6).

3. CONCLUSIONS

In summary, interactions of BLG with HP and PPIX were investigated under both alkaline and acidic conditions (pH 7.4 and 6.2) in order to explore the potential of BLG acting as the pH-sensitive carriers for these drugs. The fluorescence quenching analyses reveal that the static quenching is dominant, resulting in the formations of HP-BLG and PPIX-BLG complexes. In addition, the results of CD spectra and UV−vis studies indicate that the secondary structures of BLG are changed after binding HP or PPIX, and FRET analyses reveal that resonance energy transfer could occur between HP/PPIX and BLG, which also confirm the formations of complexes. The thermodynamic parameters show that the formations of these two complexes are spontaneous and endothermic processes, in which hydrophobic force is the main acting force. Furthermore, these data also display that the binding sites of HP to BLG might be different from that of PPIX to BLG, and a highly possible reason is the opening−closure states of the EF loop under different pH values, determining the accessibility to the central hydrophobic cavity of the β-barrel. This hypothesis is confirmed by molecular docking and ANS binding analyses. The results indicate that the central hydrophobic cavity of the β-barrel is available for HP binding only when the EF loop is opened (pH 7.4), while the binding sites of HP are just located on the external surface of BLG when the EF loop is closed (pH 6.2). Additionally, the binding sites of PPIX are both located on the external surface of BLG, which are less dependent on pH values. This work could provide a new insight into the mechanisms of noncovalent interactions between BLG and HP/PPIX. It also suggests the potential application values of BLG in designing pH-sensitive carriers for the delivery of poorly soluble drugs, in which BLG could be used as a carrier or part of a carrier.

4. EXPERIMENTAL METHODS

4.1. Materials. Bovine milk BLG (purity >90%) and ANS (8-anilino-1-naphthalenesulfonate) were purchased from Sigma-Aldrich (USA). HP and PPIX were purchased from Shanghai Aladdin Biochemical Technology (China). Other reagents and materials were analytical grade and used without further purification.

4.2. Stock Solution Preparation. All the solutions were prepared using 20 mM sodium phosphate buffer solution (pH 7.4). BLG powder was dissolved into sodium phosphate buffer solution to prepare 50 μM BLG stock solution. HP was initially dissolved in pyridine to prepare 5 mM HP stock solution in pyridine, while PPIX was initially dissolved in dimethyl sulfoxide to prepare 5 mM HP stock solution in dimethyl sulfoxide. Then, the 5 mM HP stock solution in pyridine was dissolved into sodium phosphate buffer solution to yield the 50 μM HP stock solution with 1% v/v pyridine. Similarly, the 5 mM PPIX stock solution in dimethyl sulfoxide was dissolved into sodium phosphate buffer solution to yield the 50 μM PPIX stock solution with 1% v/v dimethyl sulfoxide.

4.3. Synthesis of HP-BLG and PPIX-BLG Complexes. The HP-BLG complex with different ratios of HP to BLG was prepared by adding appropriate amounts of the 50 μM BLG stock solution and 50 μM HP stock solution in sodium phosphate buffer solution. The final concentrations of BLG and HP were 5 and 0−40 μM, respectively. Similarly, the PPIX-BLG complex with different ratios of PPIX to BLG was also prepared using the same method as that for the HP-BLG complex. The HP-BLG and PPIX-BLG solutions were adjusted to pH 7.4 and 6.2 by 1 M NaOH or 1 M HCl, respectively, followed by incubating at different temperatures (27, 37, and 47 °C) for 20 min.

4.4. Characterization. Fluorescence studies were performed using a Hitachi F-4600 fluorescence spectrophotometer (Tokyo, Japan). UV−vis absorption spectra were recorded with a UV−vis spectrophotometer (UV2660, Shimadzu, Japan). Circular dichroism (CD) measurements were achieved using a Chirascan qCD spectrometer (Applied Photophysics, UK). CDNN software was utilized to analyze the secondary structure of the protein.

4.5. Molecular Docking Study. Molecular docking analyses were performed using AutoDock Vina software. The protein structures of BLG at pH 7.4 (ID: 2GJ5) and at pH 6.2 (ID: 3BLG) were obtained from the RCSB Protein Data Bank

https://doi.org/10.1021/acsomega.1c00279
ACS Omega 2021, 6, 9680−9691

(http://www.rcsb.org/pdb). BLG molecules were dehydrated and hydrotreated using AutoDockTools before docking analysis. The molecular structures of HP and PPIX were modeled using ChemDraw Professional 19 and optimized to the minimized energy states. The docking processes were performed using a grid box (20 Å × 20 Å × 20 Å) with a grid spacing of 0.375 Å followed by approaching the ligands to different sites of the BLG structure (running 10 times). The docking results were analyzed using Discovery Studio 2020.

■ ASSOCIATED CONTENT

Supporting Information

The Supporting Information is available free of charge at https://pubs.acs.org/doi/10.1021/acsomega.1c00279.

Molecular structures of HP and PPIX, and fluorescence quenching spectra (Figure S1), synchronous fluorescence spectra (Figure S2), schematic illustrations of BLG structure (Figure S3), overlaps of fluorescence spectra and UV−vis spectra (Figure S4), molecular docking analyses (Figures S5 and S6), fluorescence quenching parameters (Tables S1 and S2), CD analysis results (Tables S3 and S4), and binding parameters (Tables S5 and S6) (PDF)

■ AUTHOR INFORMATION

Corresponding Authors

Zhu Zeng − *School of Basic Medical Sciences, Guizhou Medical University, Guiyang 550025, P. R. China; Key Laboratory of Biology and Medical Engineering/Immune Cells and Antibody Engineering Research Center of Guizhou Province, School of Biology and Engineering, Guizhou Medical University, Guiyang 550025, P. R. China*; Phone: +86-0851-88174044; Email: zengzhu@gmc.edu.cn

Jin Chen − *School of Basic Medical Sciences, Guizhou Medical University, Guiyang 550025, P. R. China; Key Laboratory of Biology and Medical Engineering/Immune Cells and Antibody Engineering Research Center of Guizhou Province, School of Biology and Engineering, Guizhou Medical University, Guiyang 550025, P. R. China*; orcid.org/0000-0003-4757-512X; Phone: +86-0851-88174044; Email: chenjin_fdt@163.com

Authors

Yun Wang − *School of Basic Medical Sciences, Guizhou Medical University, Guiyang 550025, P. R. China; Key Laboratory of Biology and Medical Engineering/Immune Cells and Antibody Engineering Research Center of Guizhou Province, School of Biology and Engineering, Guizhou Medical University, Guiyang 550025, P. R. China*

Min Gong − *Key Laboratory of Biology and Medical Engineering/Immune Cells and Antibody Engineering Research Center of Guizhou Province, School of Biology and Engineering, Guizhou Medical University, Guiyang 550025, P. R. China*

Zhuo Huang − *Key Laboratory of Biology and Medical Engineering/Immune Cells and Antibody Engineering Research Center of Guizhou Province, School of Biology and Engineering, Guizhou Medical University, Guiyang 550025, P. R. China*

Hai Min − *Key Laboratory of Biology and Medical Engineering/Immune Cells and Antibody Engineering Research Center of Guizhou Province, School of Biology and Engineering, Guizhou Medical University, Guiyang 550025, P. R. China*

Peng Yu − *School of Basic Medical Sciences, Guizhou Medical University, Guiyang 550025, P. R. China; Key Laboratory of Biology and Medical Engineering/Immune Cells and Antibody Engineering Research Center of Guizhou Province, School of Biology and Engineering, Guizhou Medical University, Guiyang 550025, P. R. China*

Fuzhou Tang − *Key Laboratory of Biology and Medical Engineering/Immune Cells and Antibody Engineering Research Center of Guizhou Province, School of Biology and Engineering, Guizhou Medical University, Guiyang 550025, P. R. China*

Yuannong Ye − *Key Laboratory of Biology and Medical Engineering/Immune Cells and Antibody Engineering Research Center of Guizhou Province, School of Biology and Engineering, Guizhou Medical University, Guiyang 550025, P. R. China*

Simian Zhu − *School of Basic Medical Sciences, Guizhou Medical University, Guiyang 550025, P. R. China; Key Laboratory of Biology and Medical Engineering/Immune Cells and Antibody Engineering Research Center of Guizhou Province, School of Biology and Engineering, Guizhou Medical University, Guiyang 550025, P. R. China*

Zuquan Hu − *School of Basic Medical Sciences, Guizhou Medical University, Guiyang 550025, P. R. China; Key Laboratory of Biology and Medical Engineering/Immune Cells and Antibody Engineering Research Center of Guizhou Province, School of Biology and Engineering, Guizhou Medical University, Guiyang 550025, P. R. China*

Complete contact information is available at: https://pubs.acs.org/10.1021/acsomega.1c00279

Author Contributions

#Y.W. and M.G. contributed equally to this work. The manuscript was written through contributions of all authors. All authors have given approval to the final version of the manuscript.

Notes

The authors declare no competing financial interest.

■ ACKNOWLEDGMENTS

This work is supported by the National Natural Science Foundation of China (31860262), the China Postdoctoral Science Foundation (2019 M653492), the Guizhou Provincial Natural Science Foundation ([2017]5718, [2020]1Y091, [2018]5779-54, [2019]2787, [2018]1133, [2018]1412, and [2016]5676), the Guizhou Provincial Health Commission Science and Technology Foundation (gzwjkj2020-1-243), and the Natural Science Foundation of Education Department of Guizhou Province (KY [2021]179, KY [2021]176, and KY [2021]159).

■ REFERENCES

(1) de Rosa, A.; Naviglio, D.; di Luccia, A. Advances in photodynamic therapy of cancer. *Curr. Cancer Ther. Rev.* **2011**, *7*, 234−247.

(2) Waghorn, P. A. Radiolabelled porphyrins in nuclear medicine. *J. Labelled Compd. Radiopharm.* **2014**, *57*, 304−309.

(3) Kou, J.; Dou, D.; Yang, L. Porphyrin photosensitizers in photodynamic therapy and its applications. *Oncotarget* **2017**, *8*, 81591−81603.

(4) Rinco, O.; Brenton, J.; Douglas, A.; Maxwell, A.; Henderson, M.; Indrelie, K.; Wessels, J.; Widin, J. The effect of porphyrin structure on binding to human serum albumin by fluorescence spectroscopy. *J. Photochem. Photobiol., A* **2009**, *208*, 91−96.
(5) Qian, K.; Chen, H.; Qu, C.; Qi, J.; Du, B.; Ko, T.; Xiang, Z.; Kandawa-Schulz, M.; Wang, Y.; Cheng, Z. Mitochondria-targeted delocalized lipophilic cation complexed with human serum albumin for tumor cell imaging and treatment. *Nanomedicine* **2020**, *23*, 102087.
(6) Nagati, V.; Nakkka, S.; Yeggoni, D. P.; Subramanyam, R. Forskolin-loaded human serum albumin nanoparticles and its biological importance. *J. Biomol. Struct. Dyn.* **2020**, *38*, 1539−1550.
(7) Kessel, D. Photodynamic therapy: a brief history. *J. Clin. Med.* **2019**, *8*, 1581.
(8) Pu, Y.; Chen, W.; Yu, Z. Research progress of hemoporfin - part one: preclinical study. *Photodiagn. Photodyn. Ther.* **2012**, *9*, 180−185.
(9) Li, S.; Xiong, N.; Peng, Y.; Tang, K.; Bai, H.; Lv, X.; Jiang, Y.; Qin, X.; Yang, H.; Wu, C.; Zhou, P.; Liu, Y. Acidic pH*e* regulates cytoskeletal dynamics through conformational integrin β1 activation and promotes membrane protrusion. *Biochim. Biophys. Acta, Mol. Basis Dis.* **2018**, *1864*, 2395−2408.
(10) Webb, B. A.; Chimenti, M.; Jacobson, M. P.; Barber, D. L. Dysregulated pH: a perfect storm for cancer progression. *Nat. Rev. Cancer* **2011**, *11*, 671−677.
(11) Loch, J. I.; Bonarek, P.; Lewiński, K. Conformational flexibility and ligand binding properties of ovine β-lactoglobulin. *Acta Biochim. Pol.* **2019**, *66*, 577−584.
(12) Tavel, L.; Moreau, C.; Bouhallab, S.; Li-Chan, E. C. Y.; Guichard, E. Interactions between aroma compounds and β-lactoglobulin in the heat-induced molten globule state. *Food Chem.* **2010**, *119*, 1550−1556.
(13) Zsila, F.; Hazai, E.; Sawyer, L. Binding of the pepper alkaloid piperine to bovine β-lactoglobulin: circular dichroism spectroscopy and molecular modeling study. *J. Agric. Food Chem.* **2005**, *53*, 10179−10185.
(14) al-Shabib, N. A.; Khan, J. M.; Malik, A.; Tabish Rehman, M.; AlAjmi, M. F.; Husain, F. M.; Hisamuddin, M.; Altwaijry, N. Molecular interaction of tea catechin with bovine β-lactoglobulin: a spectroscopic and in silico studies. *Saudi Pharm. J.* **2020**, *28*, 238−245.
(15) Ghalandari, B.; Divsalar, A.; Saboury, A. A.; Parivar, K. β-lactoglobulin nanoparticle as a chemotherapy agent carrier for oral drug delivery system. *J. Iran. Chem. Soc.* **2015**, *12*, 613−619.
(16) Shafaei, Z.; Ghalandari, B.; Vaseghi, A.; Divsalar, A.; Haertlé, T.; Saboury, A. A.; Sawyer, L. β-lactoglobulin: an efficient nanocarrier for advanced delivery systems. *Nanomedicine* **2017**, *13*, 1685−1692.
(17) Świątek, S.; Komorek, P.; Turner, G.; Jachimska, B. β-lactoglobulin as a potential carrier for bioactive molecules. *Bioelectrochemistry* **2019**, *126*, 137−145.
(18) Hendler, N.; Belgorodsky, B.; Mentovich, E. D.; Richter, S.; Fadeev, L.; Gozin, M. Multiple self-assembly functional structures based on versatile binding sites of β-lactoglobulin. *Adv. Funct. Mater.* **2012**, *22*, 3765−3776.
(19) Wang, C.; Zhou, X.; Wang, H.; Sun, X.; Guo, M. Interactions between β-lactoglobulin and 3,3′-diindolylmethane in model system. *Molecules* **2019**, *24*, 2151.
(20) Mehraban, M. H.; Odooli, S.; Yousefi, R.; Roghanian, R.; Motovali-Bashi, M.; Moosavi-Movahedi, A. A.; Ghasemi, Y. The interaction of beta-lactoglobulin with ciprofloxacin and kanamycin; a spectroscopic and molecular modeling approach. *J. Biomol. Struct. Dyn.* **2017**, *35*, 1968−1978.
(21) Wang, R.; Liu, Y.; Hu, X.; Pan, J.; Gong, D.; Zhang, G. New insights into the binding mechanism between osthole and β-lactoglobulin: spectroscopic, chemometrics and docking studies. *Food Res. Int.* **2019**, *120*, 226−234.
(22) Agudelo, D.; Bérubé, G.; Tajmir-Riahi, H. A. An overview on the delivery of antitumor drug doxorubicin by carrier proteins. *Int. J. Biol. Macromol.* **2016**, *88*, 354−360.
(23) Liang, L.; Subirade, M. β-lactoglobulin/folic acid complexes: formation, characterization, and biological implication. *J. Phys. Chem. B* **2010**, *114*, 6707−6712.
(24) Hashempour, S.; Shahabadi, N.; Adewoye, A.; Murphy, B.; Rouse, C.; Salvatore, B. A.; Stratton, C.; Mahdavian, E. Binding studies of AICAR and human serum albumin by spectroscopic, theoretical, and computational methodologies. *Molecules* **2020**, *25*, 5410.
(25) Roufegarinejad, L.; Amarowicz, R.; Jahanban-Esfahlan, A. Characterizing the interaction between pyrogallol and human serum albumin by spectroscopic and molecular docking methods. *J. Biomol. Struct. Dyn.* **2019**, *37*, 2766−2775.
(26) Jahanban-Esfahlan, A.; Davaran, S.; Moosavi-Movahedi, A. A.; Dastmalchi, S. Investigating the interaction of juglone (5-hydroxy-1, 4-naphthoquinone) with serum albumins using spectroscopic and in silico methods. *J. Iran. Chem. Soc.* **2017**, *14*, 1527−1540.
(27) Zimet, P.; Livney, Y. D. Beta-lactoglobulin and its nanocomplexes with pectin as vehicles for ω-3 polyunsaturated fatty acids. *Food Hydrocolloids* **2009**, *23*, 1120−1126.
(28) Ghalandari, B.; Divsalar, A.; Saboury, A. A.; Haertlé, T.; Parivar, K.; Bazl, R.; Eslami-Moghadam, M.; Amanlou, M. Spectroscopic and theoretical investigation of oxali-palladium interactions with β-lactoglobulin. *Spectrochim. Acta, Part A* **2014**, *118*, 1038−1046.
(29) Zhang, M.-F.; Xu, Z.-Q.; Ge, Y.-S.; Jiang, F.-L.; Liu, Y. Binding of fullerol to human serum albumin: spectroscopic and electrochemical approach. *J. Photochem. Photobiol., B* **2012**, *108*, 34−43.
(30) Ghalandari, B.; Divsalar, A.; Eslami-Moghadam, M.; Saboury, A. A.; Haertlé, T.; Amanlou, M.; Parivar, K. Probing of the interaction between β-lactoglobulin and the anticancer drug oxaliplatin. *Appl. Biochem. Biotechnol.* **2015**, *175*, 974−987.
(31) Sharma, A.; Ghosh, K. S. Studies on molecular interactions between bovine β-lactoglobulin and silver nanoparticles. *Protein Pept. Lett.* **2020**, *27*, 793−800.
(32) Paul, B. K.; Ghosh, N.; Mukherjee, S. Binding interaction of a prospective chemotherapeutic antibacterial drug with β-lactoglobulin: results and challenges. *Langmuir* **2014**, *30*, 5921−5929.
(33) Ghosh, N.; Mondal, R.; Mukherjee, S. Inverse temperature dependence in static quenching versus calorimetric exploration: binding interaction of chloramphenicol to β-lactoglobulin. *Langmuir* **2015**, *31*, 8074−8080.
(34) Jahanban-Esfahlan, A.; Panahi-Azar, V. Interaction of glutathione with bovine serum albumin: spectroscopy and molecular docking. *Food Chem.* **2016**, *202*, 426−431.
(35) Roufegarinejad, L.; Jahanban-Esfahlan, A.; Sajed-Amin, S.; Panahi-Azar, V.; Tabibiazar, M. Molecular interactions of thymol with bovine serum albumin: spectroscopic and molecular docking studies. *J. Mol. Recognit.* **2018**, *31*, No. e2704.
(36) Agudelo, D.; Beauregard, M.; Bérubé, G.; Tajmir-Riahi, H.-A. Antibiotic doxorubicin and its derivative bind milk β-lactoglobulin. *J. Photochem. Photobiol., B* **2012**, *117*, 185−192.
(37) Yang, L.; Huo, D.; Hou, C.; Yang, M.; Fa, H.; Luo, X. Interaction of monosulfonate tetraphenyl porphyrin (H_2TPPS_1) with plant-esterase: determination of the binding mechanism by spectroscopic methods. *Spectrochim. Acta, Part A* **2011**, *78*, 1349−1355.
(38) Chen, T.; Zhu, X.; Chen, Q.; Ge, M.; Jia, X.; Wang, X.; Ge, C. Interaction between Z-ligustilide from radix angelica sinensis and human serum albumin. *Food Chem.* **2015**, *186*, 292−297.
(39) He, W.; Li, Y.; Xue, C.; Hu, Z.; Chen, X.; Sheng, F. Effect of Chinese medicine alpinetin on the structure of human serum albumin. *Bioorg. Med. Chem.* **2005**, *13*, 1837−1845.
(40) Hemmateenejad, B.; Shamsipur, M.; Samari, F.; Khayamian, T.; Ebrahimi, M.; Rezaei, Z. Combined fluorescence spectroscopy and molecular modeling studies on the interaction between harmalol and human serum albumin. *J. Pharm. Biomed. Anal.* **2012**, *67-68*, 201−208.
(41) Rabbani, G.; Baig, M. H.; Jan, A. T.; Ju Lee, E.; Khan, M. V.; Zaman, M.; Farouk, A.-E.; Khan, R. H.; Choi, I. Binding of erucic acid with human serum albumin using a spectroscopic and molecular docking study. *Int. J. Biol. Macromol.* **2017**, *105*, 1572−1580.

https://doi.org/10.1021/acsomega.1c00279
ACS Omega 2021, 6, 9680−9691

(42) Jayabharathi, J.; Thanikachalam, V.; Srinivasan, N.; Venkatesh Perumal, M. Luminescent study on the binding interaction of bioactive imidazole with bovine serum albumin - a static quenching mechanism. *Spectrochim. Acta, Part A* **2011**, *84*, 233−237.
(43) Bello, M.; García-Hernández, E. Ligand entry into the calyx of β-lactoglobulin. *Biopolymers* **2014**, *101*, 744−757.
(44) Moro, A.; Báez, G. D.; Busti, P. A.; Ballerini, G. A.; Delorenzi, N. J. Effects of heat-treated β-lactoglobulin and its aggregates on foaming properties. *Food Hydrocolloids* **2011**, *25*, 1009−1015.
(45) Sardar, S.; Anas, M.; Maity, S.; Pal, S.; Parvej, H.; Begum, S.; Dalui, R.; Sepay, N.; Halder, U. C. Silver nanoparticle modulates the aggregation of beta-lactoglobulin and induces to form rod-like aggregates. *Int. J. Biol. Macromol.* **2019**, *125*, 596−604.

https://doi.org/10.1021/acsomega.1c00279
ACS Omega 2021, 6, 9680−9691